

Received February 8, 2021, accepted February 16, 2021, date of publication February 22, 2021, date of current version March 3, 2021.

Digital Object Identifier 10.1109/ACCESS.2021.3061141

# Differential Flatness-Based Performance Enhancement of a Vector Controlled VSC With an LCL-Filter for Weak Grids

HASSAN ABDULLAH KHALID<sup>1</sup>, CARLO CECATI<sup>2</sup>, (Fellow, IEEE),  
NASSER AHMED AL-EMADI<sup>3</sup>, (Member, IEEE),  
ADEL GASTLI<sup>3</sup>, (Senior Member, IEEE),  
AND LAZHAR BEN-BRAHIM<sup>3</sup>, (Senior Member, IEEE)

<sup>1</sup>Center for Advanced Studies in Energy, National University of Science and Technology, Islamabad 44000, Pakistan

<sup>2</sup>Department of Information Engineering, Computer Science and Mathematics, University of L'Aquila, 67100 L'Aquila, Italy

<sup>3</sup>Department of Electrical Engineering, Qatar University, Doha, Qatar

Corresponding author: Adel Gastli (adel.gastli@qu.edu.qa)

This work was supported by the Qatar National Library.

**ABSTRACT** In this paper, a novel single-loop flatness-based controller (FBC) is proposed to control the grid-side current in a shunt converter connected to a weak grid through an LCL-filter. After its mathematical description, the paper reports controller implementation and some performance comparisons with two distinct implementations of the widely diffused vector current control approach, during balanced and unbalanced grid voltages, and weak grid conditions. Obtained results highlight higher tracking capability and better dynamic response of the proposed FBC. Moreover, because of its reduced negative conductance region, unstable behaviors that can be observed in weak grids appear significantly improved due to a reduced influence of the phase-locked loop system.


**INDEX TERMS** Flatness-based control, LCL-filter, vector current control, voltage source converter, weak grids.

## I. INTRODUCTION

The increasing penetration of Distributed Generation (DG) [1] in today's power systems has led to a considerable amount of voltage source converters (VSC) such as photovoltaic and wind generators [2] connected to the grid, thus, leading to efficiency reductions, grid impedance fluctuation, and increased failure rates, especially in low voltage distribution grids [3]. Typical VSC is shunt connected on the grid, with the interposition of an output filter, as shown in Fig. 1. LCL-filter is often considered a good choice as it provides a high level of harmonics attenuation with the minimum component size and with satisfactory grid decoupling [4]. However, if not well designed it introduces resonances which are usually handled by the controller itself through either active damping i.e. through a virtual resistor or

an observer [5], [6], or passive damping, i.e. through physical resistor [7].

Several controllers dealing with shunt-connected VSC with LCL-filter have been proposed in the literature, many based on the Vector Current Control (VCC) concept, that uses the synchronous rotating frame of reference and a decoupled proportional-integral (PI) controller [8], [9]. However, bandwidth and robustness are quite limited as the third-order LCL-filter introduces overshoots and resonances [10]. If the grid impedance increases, as in weak grids, increased interaction between the phase-locked loop (PLL) and the VCC can be observed, which leads to harmonics problems and potential instability [11]–[13]. To increase robustness and performance, more sophisticated controllers other than PI have been proposed in the literature, which makes use of observers, sliding-mode control, active filters, fuzzy-logic control, passivity-based control among other techniques [14]–[21]. However, fewer studies have considered the impact of ultra-weak grids, i.e. those where the short circuit ratio (SCR)

The associate editor coordinating the review of this manuscript and approving it for publication was Ali Raza .

is less than two, where the interactions between the PLL and the current controller appear as discussed in [22], [23].

As a possible solution, this paper presents a novel flatness-based controller (FBC) that considerably improves the performance of the VCC by using the flatness property of the non-linear systems [24]. Flatness-based control doesn't transform a non-linear system into a linear one through a change in variables, but while conserving all the nonlinearities of the system offers fast system response with limited overshoots and oscillations [25]. It has been successfully applied to many applications and in different fields, including electric drives, rectifiers, and inverters, and more recently, grid-connected converters [26]–[29]. For instance, an open-loop flatness-based control for an isolated inverter with an LC-filter has been proposed in [30], highlighting superior dynamic response, better total harmonic distortion (THD), and higher robustness than conventional VCCs. It has also been applied and experimentally verified with a DSTATCOM employing an L-filter, obtaining good step response and robustness under unbalanced conditions [31]; however, controller performance has not been evaluated under real grid conditions and during impedance variations, which always contains harmonics. In [32], an adaptive flatness based current controller has been studied for DSTATCOM with L-filter that can automatically tune itself under different grid operating conditions. However, its performance has not been investigated in presence of grid harmonics, unbalances and weak grid conditions. A dual flatness-based controller with LCL-filter has been proposed by authors in [33], but it requires a current injection and the introduction of a capacitor voltage feedback hence extra sensors, significant controller complexity and high cost.

This paper proposes a novel FBC for grid-connected VSC with an LCL output filter for grid-side current control, which is capable to provide smooth transient response and simple implementation. Its performance has been evaluated through simulations and experiments carried out under balanced, unbalanced, and weak grid conditions. Standard PI-based VCC controller has been chosen for comparison purposes under weak grid conditions, for which the interaction between the PLL and current controller brings the system instability. In this study, the health of the grid (weak/strong) is defined by an SCR ratio at the PCC.

The paper is organized as follows: Section II introduces the mathematical model of the system, then, after a brief discussion about PI controllers implementation, Section III, proposes a FBC applied to shunt connected VSC. Section IV compares simulation results at different SCR ratios for strong and weak grid cases. Sensitivity to inaccurate knowledge of system parameters is then discussed for FBC. Section V presents the experimental setup adopted for the controller. Results with FBC are compared with those of PI controllers with applied active and reactive current steps under strong/weak grid conditions, for ideal grid voltage and with voltage unbalance in the grid. Finally, the performance of the proposed FBC and PI controllers are evaluated under

a weak grid conditions. Some conclusions are given in Section VI.

## II. MATHEMATICAL MODEL

A schematic diagram of a shunt-connected VSC system including an LCL output filter is shown in Fig. 1. The capacitor voltage and inductor current are state variables. The model of the circuit in  $\alpha\beta$ -frame can be written as:

$$C_f \frac{d}{dt} \underline{u}_c^{\alpha\beta}(t) = \underline{i}_r^{\alpha\beta}(t) - \underline{i}_j^{\alpha\beta}(t) \quad (1)$$

where  $\underline{u}_c$  indicates the  $\alpha\beta$  voltage vector across capacitor  $C_f$ ,  $\underline{i}_r$  is the  $\alpha\beta$  current vector flowing across filter reactor  $L_{r1}$  and  $\underline{i}_j$  is the current vector across filter inductor  $L_{r2}$ , which is also injected into the grid. Notice that  $\underline{u}_c$ ,  $\underline{i}_r$  and  $\underline{i}_j$  are complex quantities.

The derivation of the converter voltage  $\underline{u}$ , can be obtained by applying Kirchhoff's Voltage Law (KVL) to the VSC output filter, which in  $\alpha\beta$  coordinate system can be written as:

$$\underline{u}^{\alpha\beta}(t) - \underline{u}_c^{\alpha\beta}(t) - R_{r1} \underline{i}_r^{\alpha\beta}(t) - L_{r1} \frac{d}{dt} \underline{i}_r^{\alpha\beta}(t) = 0 \quad (2)$$

$$\underline{e}_g^{\alpha\beta}(t) - \underline{u}_c^{\alpha\beta}(t) + R_{r2} \underline{i}_j^{\alpha\beta}(t) + L_{r2} \frac{d}{dt} \underline{i}_j^{\alpha\beta}(t) = 0 \quad (3)$$

By using a PLL circuit synchronized with the grid voltage vector, it is possible to transform from  $\alpha\beta$  to  $dq$  coordinate system, obtaining:

$$\underline{i}_r^{dq}(t) = C_f \frac{d}{dt} \underline{u}_c^{dq}(t) + \underline{i}_j^{dq}(t) + i\omega C_f \underline{u}_c^{dq}(t) \quad (4)$$

where  $i$  designates the imaginary coordinate in the complex plane and  $\omega$  is the angular frequency of the rotating  $dq$ -frame.

Applying  $\alpha\beta$  to  $dq$ -transformation to (2) and (3) yields:

$$\underline{u}^{dq}(t) = \underline{u}_c^{dq}(t) + R_{r1} \underline{i}_r^{dq}(t) + L_{r1} \frac{d}{dt} \underline{i}_r^{dq}(t) + i\omega L_{r1} \underline{i}_r^{dq}(t) \quad (5)$$

$$\underline{u}_c^{dq}(t) = \underline{e}_g^{dq}(t) + R_{r2} \underline{i}_j^{dq}(t) + L_{r2} \frac{d}{dt} \underline{i}_j^{dq}(t) + i\omega L_{r2} \underline{i}_j^{dq}(t) \quad (6)$$

## III. CURRENT CONTROLLER DESIGN

### A. VECTOR CURRENT CONTROL

#### 1) CONVERTER-SIDE PI (CPI)

In this section, a proportional-integral current controller is designed, that independently controls the  $d$  and  $q$  components of the filter current  $\underline{i}_r^{dq}(t)$ , i.e. the active and reactive currents injected at the capacitor connection point as shown in Fig. 1. The PLL is synchronized with the capacitor voltage vector. For the dynamic model in (5), using the Internal Model Control (IMC) approach [34], the PI current controller in discrete time  $k$  is given by:

$$\begin{aligned} \underline{u}^{dq*}(k) = & \underline{u}_c^{dq}(k) + i\omega L_{r1} \underline{i}_r^{dq}(k) + \alpha_{cc} L_{r1} \left( \underline{i}_r^{dq*}(k) - \underline{i}_r^{dq}(k) \right) \\ & + \alpha_{cc} R_{r1} T_s \sum_{n=0}^k \left( \underline{i}_r^{dq*}(n) - \underline{i}_r^{dq}(n) \right) \quad (7) \end{aligned}$$

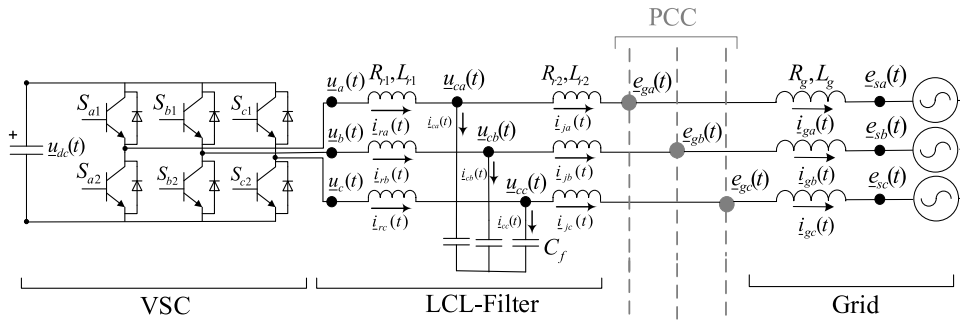


FIGURE 1. Three-phase shunt connected two-level VSC with an LCL-filter.

where  $\alpha_{cc}$  represents the desired closed-loop bandwidth of the current controller on the converter-side, and the superscript “\*” denotes a reference signal.

To deal with system parameter variations, disturbances and resonance, active damping must be included in (7). This involves calculating controller parameters assuming a fictitious resistance ( $R_a$ ) in the system and will impact the value of the total system resistance which is equal to  $R_{r1} + R_a$ . The value of the active damping term should be selected carefully. Even if a high value would provide large damping to system disturbances, the increase of the integral gain might lead to instability when used in discrete controllers with non-negligible time delays. Explanation and guidelines on the selection of active damping can be found in [35]. By adding the active damping compensation to the current controller in (7), the PI current controller is now given by:

$$\begin{aligned} \underline{u}^{dq*}(k) &= (i\omega L_{r1} - R_a) \underline{i}_r^{dq*}(k) + \alpha_{cc} L_{r1} \left( \underline{i}_r^{dq*}(k) - \underline{i}_r^{dq}(k) \right) \\ &+ \underline{u}_c^{dq}(k) + \alpha_{cc} (R_{r1} + R_a) \\ &\times T_s \sum_{n=0}^k \left( \underline{i}_r^{dq*}(n) - \underline{i}_r^{dq}(n) \right) \end{aligned} \quad (8)$$

The controller gains have been calculated as:  $k_{pc} = \alpha_{cc} L_{r1}$ ,  $k_{ic} = \alpha_{cc} (R_{r1} + R_a)$  and for  $P_a\%$  active damping:  $R_a = \frac{P_a}{100} (k_p - R_{r1})$ . Note that increasing the damping will increase the integrator gain and will reduce the stability margins. Here,  $\alpha_{cc}$  has been set at 2513 rad/s with 10% damping.

## 2) GRID-SIDE PI (GPI)

A PI controller has been designed to independently control the  $d$  and  $q$  components of the filter current  $\underline{i}_j^{dq}(t)$  that represents the active and reactive current injected at the PCC, respectively, as shown in Fig. 1. For the dynamic model in (6), the already mentioned IMC approach has been used. The discretized PI current controller is given by:

$$\begin{aligned} \underline{u}_g^{dq*}(k) &= \underline{e}_g^{dq}(k) + i\omega L_{r2} \underline{i}_j^{dq}(k) + \alpha_{cg} L_{r2} \left( \underline{i}_j^{dq*}(k) - \underline{i}_j^{dq}(k) \right) \\ &+ \alpha_{cg} R_{r2} T_s \sum_{n=0}^k \left( \underline{i}_j^{dq*}(n) - \underline{i}_j^{dq}(n) \right) \end{aligned} \quad (9)$$

where  $\alpha_{cg}$  represents the desired closed-loop bandwidth of the current controller on the grid-side, and the superscript “\*”

denotes a reference signal. The controller gains have been calculated as:  $k_{pg} = \alpha_{cg} L_{r2}$  and  $k_{ig} = \alpha_{cg} R_{r2}$  rad/s. Here,  $\alpha_{cg}$  has been set at 2513 rad/s.

For the active damping of LCL-filter resonance, in a grid-connected VSC with only grid-current feedback control, a negative HPF has been employed that introduces a virtual impedance across the grid-side inductance [36]. This added impedance is more precisely represented by a series RL branch in parallel with a negative inductance that helps to mitigate phase lag caused by time delays, which is common in a digitally control. The transfer function of the HPF is therefore given as:

$$\begin{aligned} G_{ad}(s) &= -\frac{k_{ad}s}{s + \omega_{ad}} \\ k_{ad} &= L_{r1} L_{r2} R_v / L_v^2; \quad \omega_{ad} = R_v / L_v \end{aligned} \quad (10)$$

where  $\omega_{ad}$  and  $k_{ad}$  are cutoff frequency and gain of the HPF, respectively, while  $L_v$  and  $R_v$  are inductance and resistance of the virtual impedance across the grid-side. Note that the selection of both the HPF gain and cutoff frequency has been based on the guidelines given in [36] and are selected as:  $k_{ad} = 25$  and  $\omega_{ad} = 10.9$  rad/s.

The open-loop bode plots for both the CPI and GPI controllers are shown in Fig. 5 with varying grid impedance ( $L_g$ ) from 0.5 mH to 12 mH. It can be observed that the GPI has better gain and phase margins as compared to CPI for weak grids.

## B. FLATNESS BASED CONTROL

An effective control algorithm can be designed using the flatness theory as described in [37]. For a nonlinear system  $\dot{x} = f(x, u)$ , with state vector:  $x = (x_1, x_2, \dots, x_r)$  and control vector:  $u = (u_1, u_2, \dots, u_m)$ , where  $m \leq n$ , is differentially flat if and only if there exists a vector:  $y = (y_1, y_2, \dots, y_m)$  such that:

- $y$  and its successive derivatives  $\dot{y}, \ddot{y}, \dots$  are independent,
- $y = h(x, u, \dot{u}, \dots, u^r)$  gives generalized output,
- Conversely,  $x$  and  $u$  can be expressed as:  $x = \varphi(y, \dot{y}, \dots, y^{\alpha})$ ,  $u = \psi(y, \dot{y}, \dots, y^{\alpha+1})$  with  $\dot{\varphi} \equiv f(\varphi, \psi)$ . Then the vector  $y$  is called flat output.

In this paper, a flatness-based control is proposed for shunt connected VSC with an LCL-filter. The proposed controller

in Fig. 3 consists of two parallel control blocks: Flatness Block (FB) and Secondary PI Regulator (SPIR). The FB is an open-loop controller that is based on the model of a system using the flatness theory that conserves all the nonlinearities of the system. The additional parallel SPIR is a feedback controller that minimizes the error due to unmodeled nonlinearities in the system.

### 1) PROOF OF FLAT SYSTEM

Representing the system equations as  $\dot{x} = f(x, u)$  by rewriting (4), (5) and (6), gives

$$L_{r2} \frac{d}{dt} i_j^{dq}(t) = -R_r 2 i_j^{dq}(t) - i\omega L_{r2} i_j^{dq}(t) + \underline{u}_c^{dq}(t) - \underline{e}_g^{dq}(t) \quad (11)$$

$$C_f \frac{d}{dt} \underline{u}_c^{dq}(t) = i_r^{dq}(t) - i_j^{dq}(t) - i\omega C_f \underline{u}_c^{dq}(t) \quad (12)$$

$$L_{r1} \frac{d}{dt} i_r^{dq}(t) = -\underline{u}_c^{dq}(t) - R_{r1} i_r^{dq}(t) + \underline{u}_c^{dq}(t) - i\omega L_{r1} i_r^{dq}(t) \quad (13)$$

where the state vector is  $x = (i_j^{dq}, \underline{u}_c^{dq}, i_r^{dq})$  and the control vector is  $u = (\underline{u}^{dq})$ . Now, defining inductor  $L_2$  current  $i_j^{dq}$  as the flat variable:  $y^{dq} = i_j^{dq}$  and substituting it in (11) and (12), yields:

$$\underline{u}_c^{dq}(t) = R_r 2 y^{dq}(t) + i\omega L_{r2} y^{dq}(t) + L_{r2} \dot{y}^{dq}(t) + \underline{e}_g^{dq}(t) = \xi(y, \dot{y}) \quad (14)$$

$$i_r^{dq}(t) = y^{dq}(t) + C_f \dot{y}^{dq}(t) + i\omega C_f \underline{u}_c^{dq}(t) \quad (15)$$

Putting the expression of  $\underline{u}_c^{dq}(t)$  and its derivative in (15), yields:

$$i_r^{dq}(t) = y^{dq}(t) + C_f \dot{\xi} + i\omega C_f \xi = \varphi(y, \dot{y}, \ddot{y}) \quad (16)$$

Finally, the control output  $\underline{u}^{dq}(t)$  is represented using the flat variable  $y$  as:

$$\underline{u}_{FB}^{dq}(t) \equiv \underline{u}^{dq}(t) = \xi + R_{r1} \varphi + L_{r1} \dot{\varphi} + i\omega L_{r1} \varphi = \beta(y, \dot{y}, \ddot{y}, \ddot{\ddot{y}}) \quad (17)$$

Equation (17) proves that the system is differentially flat. In fact, it can be represented using the flat variable and its derivatives. However, for digital control implementation it needs to be discretized. Furthermore, in order to eliminate disturbances from the measured signals or other nonlinearities, a feedback loop must be integrated into the above flatness block. Here, a parallel structure is proposed, where the FB keeps the system close to the reference trajectory, while the parallel SPIR works in a very small error region to bring the steady-state error to zero, thus adding up in the final output as shown in Fig. 2. In the continuous-time domain SPIR can be represented as:

$$\underline{u}_{PI}^{dq*}(t) = k_1 (i_g^{dq*}(t) - i_g^{dq}(t)) + k_2 \int (i_g^{dq*}(t) - i_g^{dq}(t)) dt \quad (18)$$

where  $k_1$  and  $k_2$  are proportional and integrator gains, respectively, which are tuned by using the IMC method at a bandwidth of 2513 rad/s. Note that equations (14)-(18) have been

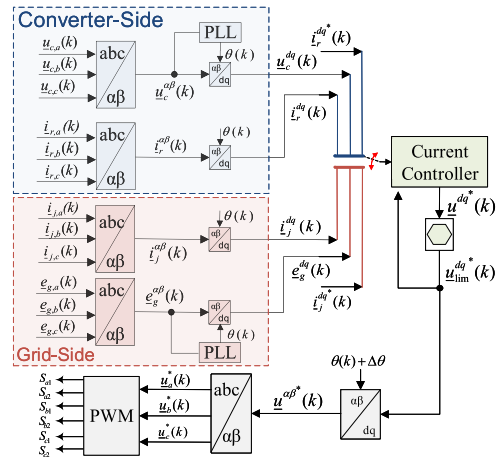


FIGURE 2. Converter and grid side current control schemes.

discretized for digital implementation. Similar to grid-side controller GPI, the proposed FBC also needs the active damping  $G_{ad}$ , as defined in (10) for resonance damping of the LCL filter.

### 2) TRAJECTORY PLANNING

Trajectory planning is the most important step for FBC implementation, as the flatness property allows all the state and input variables to be written as functions of a chosen flat output. Thus, this flat output trajectory defines all the state or input variables trajectories. Therefore, these trajectories have to be differentiable without any singularity and also be adaptable to any change in reference input signals [38]. Here, a fourth-order cascaded Butterworth filter is selected as it presents less ripples in the pass and stop bands. Thus, it generates a smoother signal in the trajectory generation blocks, as shown in Fig. 3 [39]. The cut-off frequency of this filter has been set at 1256 rad/s, which gives a 5ms smooth reference trajectory signal.

### 3) STABILITY WITHOUT CONSIDERING GRID IMPEDANCE

In this section, the stability of the proposed controller is proven. The FB is an open-loop structure that consists of three cascade loops described by (16)-(17), as shown in Fig. 3. The stability of each loop can be assessed separately, and the overall system is stable if all three loops are stable.

Splitting (11) into  $d$  and  $q$  components gives:

$$\begin{aligned} u_{cd}(k) &= e_{gd}(k) + R_{r2} y_d(k) + L_{r2} \left( \frac{y_d(k) - y_d(k-1)}{T_s} \right) \\ &\quad - \omega L_{r2} y_q(k) \\ u_{cq}(k) &= e_{gq}(k) + R_{r2} y_q(k) + L_{r2} \left( \frac{y_q(k) - y_q(k-1)}{T_s} \right) \\ &\quad + \omega L_{r2} y_d(k) \end{aligned} \quad (19)$$

and neglecting feed-forward and cross-coupling terms yields:

$$\begin{aligned} u_{cd}(k) &= R_{r2} y_d(k) + L_{r2} \left( \frac{y_d(k) - y_d(k-1)}{T_s} \right) \\ u_{cq}(k) &= R_{r2} y_q(k) + L_{r2} \left( \frac{y_q(k) - y_q(k-1)}{T_s} \right) \end{aligned} \quad (20)$$

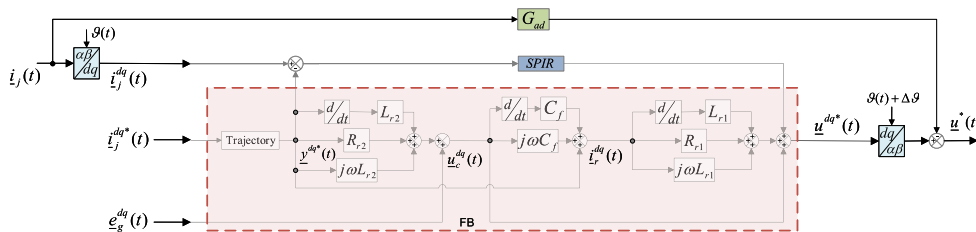


FIGURE 3. Flatness block internal diagram.

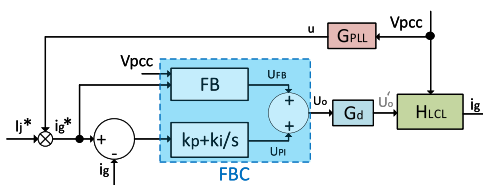


FIGURE 4. Closed loop control block diagram of the proposed FBC with LCL-filter.

$$\begin{aligned}
 u_{cd}(k) &= \frac{(T_s R_{r2} + L_{r2}) y_d(k) - L_{r2} y_d(k-1)}{T_s} \\
 u_{cq}(k) &= \frac{(T_s R_{r2} + L_{r2}) y_q(k) - L_{r2} y_q(k-1)}{T_s} \quad (21)
 \end{aligned}$$

By considering the *d*-component only, follows:

$$\begin{aligned}
 x(k+1) &= y_d(k) \\
 u_{cd}(k) &= \frac{(T_s R_{r2} + L_{r2}) y_d(k) - L_{r2} x(k)}{T_s} \quad (22)
 \end{aligned}$$

Following the same procedure for (12) and (13), and considering only the *d*-component, yields:

$$\begin{aligned}
 x(k+1) &= u_{cd}(k) \\
 i_{rd}(k) &= \frac{(C_f) u_{cd}(k) - x(k)}{T_s} \quad (23)
 \end{aligned}$$

$$u_d(k) = \frac{(T_s R_r + L_r) i_{rd}(k) - L_r x(k)}{T_s} \quad (24)$$

Using the state space form  $x(k+1) = Ax(k) + Bu(k)$ , in (22)-(24), it can be noticed that  $A = 0$ . Thus, all three cascade loops are stable and the overall system is also asymptotically stable. The stability of SPIR is similar to that of the GPI (presented in section III).

4) STABILITY WITH GRID IMPEDANCE

To show the stability of the proposed FBC in presence of grid impedance variations, the passivity-based stability analysis is used in this section. Such analysis has been widely applied to estimate the system’s external stability. Based on Fig. 6 (a), the output grid-side inductor currents are expressed as:

$$i_g = T(s) * i_g^* + Y_c * V_{pcc} \quad (25)$$

Here,  $T(s)$  denotes the reference to output closed-loop response and  $Y_c(s)$  corresponds to the VSC input admittance.

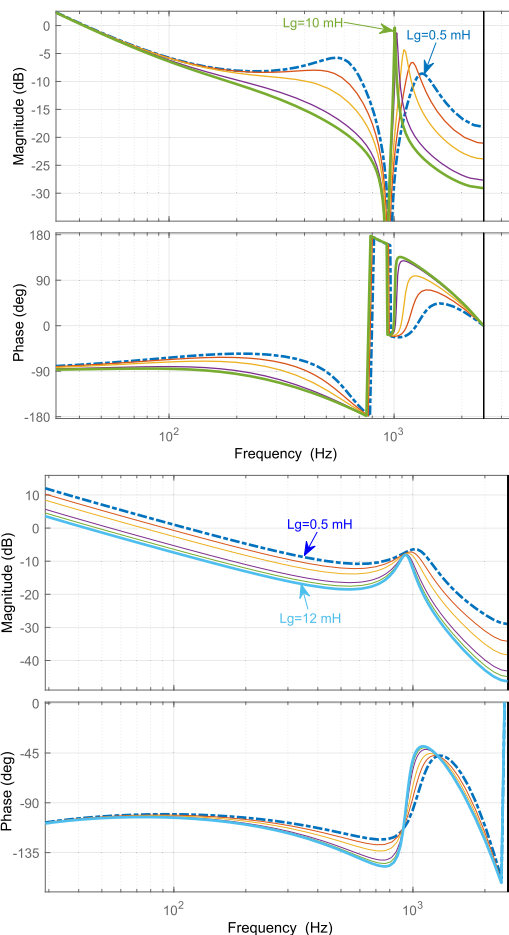
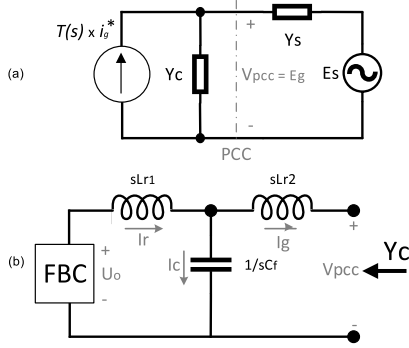


FIGURE 5. Open-loop bode diagram with plant model for CPI (top plot) and GPI (bottom plot).

Using (25), the VSC can be modeled as a combination of a controllable current source and an admittance, as shown in Fig. 6 (a). The stability of a closed-loop system depends upon both the stability of  $T(s)$  and the interaction between  $Y_c(s)$  and  $Y_s(s)$ . It is important to note that  $T(s)$  is linked with the internal stability of the VSC while the effect of a network is associated with the interaction between  $Y_c(s)$  and  $Y_s(s)$ . The impedance-based analysis of grid-connected converters has been experimentally validated in the literature where passivity theory has been used to assess the closed-loop stability conditions. The passivity property layouts the sufficient but not necessary condition for stability of interconnected



**FIGURE 6. Equivalent Models: (a) Equivalent system model of the VSC and the electrical network for impedance-based analysis and (b) equivalent circuit of  $Y_c$  calculation.**

dynamical systems. The VSC terminal response is passive for a frequency range  $[\omega_z, \omega_x]$ , if  $Y(s)$  is stable and  $|\angle Y(j\omega)| < \frac{\pi}{2}$  or  $\Re\{Y(j\omega)\} \geq 0, \forall \omega \in [\omega_z, \omega_x]$ .

As the real part of the converter admittance  $Y(s)$  corresponds to the dissipative response, a positive sign real part of  $Y_c(s)$  represents the dissipative behavior, whereas a negative sign resistance implies amplification of any oscillation at the respective frequency. The passivity of both  $Y_c(s)$  and  $Y_s(s)$  provides a sufficient condition for the stable operation of the closed-loop current controller. As  $Y_c$  is the admittance of the converter is defined as:

$$Y_c = \frac{i_g}{v_{pcc}} \quad (26)$$

then, based on Fig. 6 (b),  $Y_c$  can be calculated while considering the effect of PLL as presented in Fig. 4 and described in [40], we get:

$$Y_c = \frac{(s^2 C_f L_{r1} + s G_d C_f + 1 - G_d - I_j^* G_d G_{pll} (G_{SPIR} + G_{FB}))}{(s^3 C_f L_{r1} + s^2 G_d L_{r2} C_f + s (L_{r1} + L_{r2}) + G_{SPIR} G_d)} \quad (27)$$

In (27), the term  $G_d$  represents the overall delay in a digital control system which is defined as  $e^{-1.5T_s s}$  with a sampling time  $T_s$ . While the  $G_{pll}$  is the closed-loop transfer function of the conventional synchronous reference frame (SRF) based PLL with bandwidth  $f_{pll}$  that relates the input and estimated phases [41], given as:

$$G_{pll} = (4\pi f_{pll} + (2\pi f_{pll})^2) / (s^2 + 4\pi f_{pll} s + (2\pi f_{pll})^2)$$

Note in Fig. 4, the output of  $G_{pll}$  is  $u$  which represents the PLL output phase information of  $V_{pcc}$ . And the  $I_j^*$  is the amplitude of current reference for the FBC which is set at its rated current value for the stability analysis. The transfer functions for both the SPIR and FB are given as:

$$G_{SPIR} = \left( k_{pc} + \frac{k_{ic}}{s} \right)$$

$$G_{FB} = s^3 (L_{r1} L_{r2} C_f) + s^2 (C_f R_{r1} L_{r2} + L_{r1} C_f R_{r2}) + s (L_{r2} + C_f R_{r1} R_{r2} + L_{r1}) + R_{r1} + R_{r2}$$

**TABLE 1. System parameters.**

Grid parameters			
Grid voltage	$E_g$	173 V	1 p.u
Grid frequency	$f_g$	50 Hz	1 p.u
Line inductance	$L_g$	2-15 mH	0.116-0.873 p.u
DC-link voltage	$U_{dc}$	400 V	2.31 p.u
DC-link Capacitor	$C_{dc}$	3000 $\mu$ F	0.1965 p.u
Filter parameters			
Filter resistance	$R_{r1}$	6.2 m $\Omega$	0.0011 p.u
Filter inductance	$L_{r1}$	2 mH	0.116 p.u
Filter resistance	$R_{r2}$	5 m $\Omega$	0.00093 p.u
Filter inductance	$L_{r2}$	2 mH	0.116 p.u
Filter capacitance	$C_f$	15 $\mu$ F	39.3 p.u
Simulation/Experimental Settings			
VSC apparent power	$S_c$	4 kVA	1 p.u
Sampling frequency	$f_s$	5 kHz	100 p.u
Switching frequency	$f_{sw}$	5 kHz	100 p.u
PLL bandwidth	$f_{pll}$	20 Hz	0.4 p.u

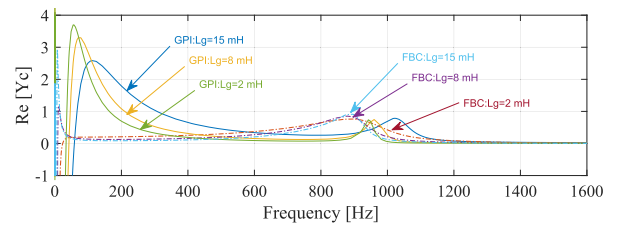


**FIGURE 7. Real part of VSC input admittance  $Y_c$ .**

By using the parameters in Table 1, the converter admittance  $Y_c$  as defined in (27) that includes the effect of PLL is presented as the real part in Fig. 6 (b) with varying frequency. It can be observed that the proposed FBC controller response presents improvements for frequencies less than 100 Hz, which is the area influenced by the PLL, resulting in an instability in weak grids for the GPI. On the other hand, the width of this negative region has been reduced, furthermore, the critical resonance frequency region between 500-1200 Hz presents improved passive damping for the proposed FBC controller as compared to GPI. Whereas, the high frequency damping remains the same for both the GPI and FBC controllers. However, passive damping has some reduction between the 100 to 500 Hz region for the proposed FBC controller which further decreases with grid impedance.

#### IV. SIMULATION RESULTS

A simulation model has been implemented in MATLAB/Simulink, for the system shown in Fig. 1. Note that, constant DC-link voltage has been assumed and PWM is used to generate the patterns for the VSC switches. A unit delay has also been introduced to take into account the delay of digital systems. The parameters used in the simulation are provided in Table 1. Three different cases are presented based on SCR values representing strong, weak and weaker grid conditions. The open-loop bode plots of both the CPI and GPI controllers are given in Fig. 5 with gains settings given in section III. The FBC controller tracking reference has been set at 1256 rad/s for 5 ms settling time.

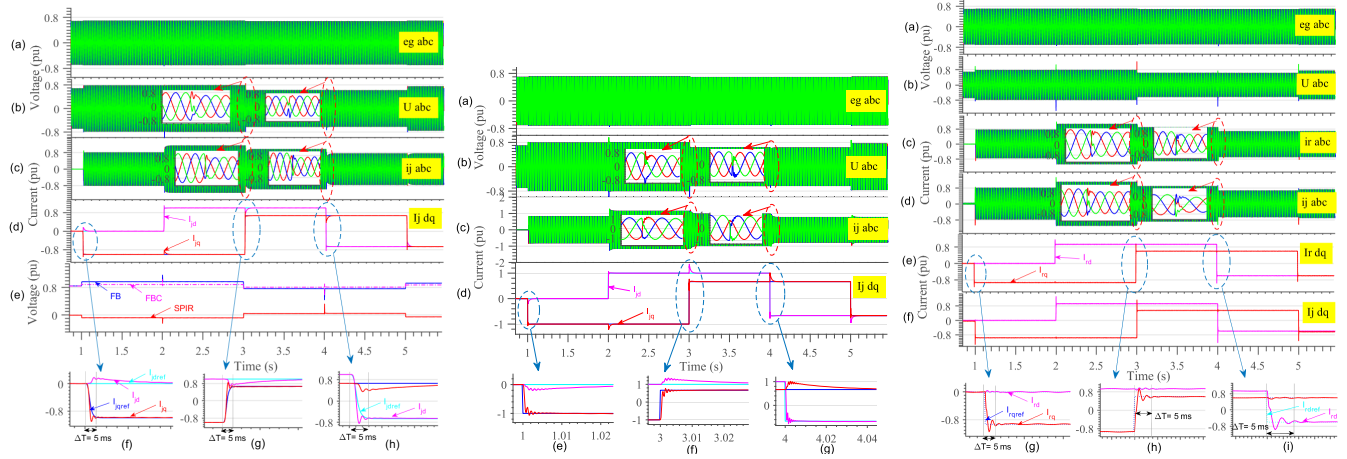


FIGURE 8. Simulation results for strong grid case (SCR = 34) with step in active and reactive currents; FBC (left plot), GPI (middle plot) and CPI (right plot).

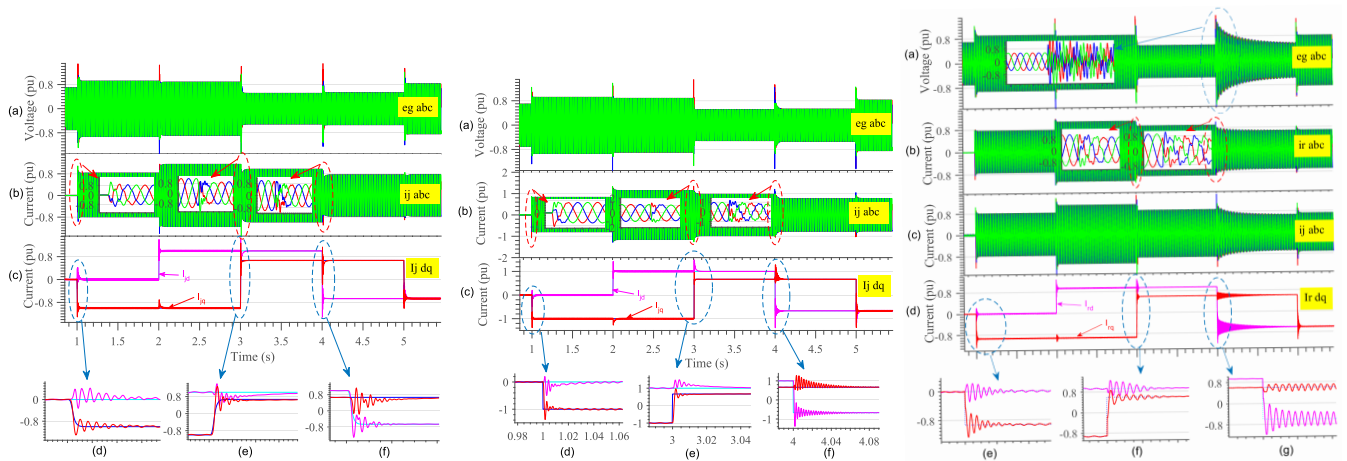


FIGURE 9. Simulation results for weak grid case (SCR = 1.7) with step in active and reactive currents; FBC (left plot), GPI (middle plot) and CPI (right plot).

TABLE 2. Simulation results with varying SCR.

L (mH)	SCR	FBC	GPI	CPI
0.5	34	stable	stable	stable
2	8.6	stable	stable	stable
4	4.3	stable	stable	stable
8	2.1	stable	stable	stable
10	1.7	stable	stable	-
12	1.4	stable	-	-
13	1.3	stable	-	-
15	1.1	-	-	-

For the strong grid case in Fig. 8, the FBC measures the  $I_{jdq}$  current smoothly follows its reference trajectory  $I_{jdqref}$  with a maximum overshoot of 0.05 p.u. and a settling time of 5 ms. For the GPI,  $I_{jdq}$  presents minor oscillations during the transients (at  $t = 1, 3$  and  $4$  s) with an overshoot of 0.02 p.u. at 3 s and a settling time of 5 ms. Compared to the above two controllers, the CPI presents a larger overshoot up to 0.3 p.u. (at  $t = 1, 2, 3$  and  $4$  s) achieving the similar settling time of 5 ms. The improved response of the proposed

FBC structure is due to the differential flatness-based open-loop controller in parallel to the SPIR that takes the reference trajectory dq-components as input signals. The incorporated SPIR removes the steady-state error between the reference and measured injected currents, as presented in 8 (e), where the FBC consists of the sum of FB and SPIR. Thus, the SPIR operates in a very narrow region as the FB keeps the system close to the reference trajectory.

Now, as the grid becomes weak at  $SCR = 1.7$ , as shown in Fig. 9, the injected current has more effect on the grid voltage at the PCC, where the PLL is also synchronized. Hence, a closed-loop is formed between the PLL and the respective current controller which is beginning to affect the stability of these controllers. Although both the FBC and GPI remain stable, there are higher oscillations at  $t = 4$  s for the GPI and an unstable operation is observed for the CPI controller. Under such conditions, the integrator gain of the CPI current controller should be reduced [42] but this slows down the controller response during transients.

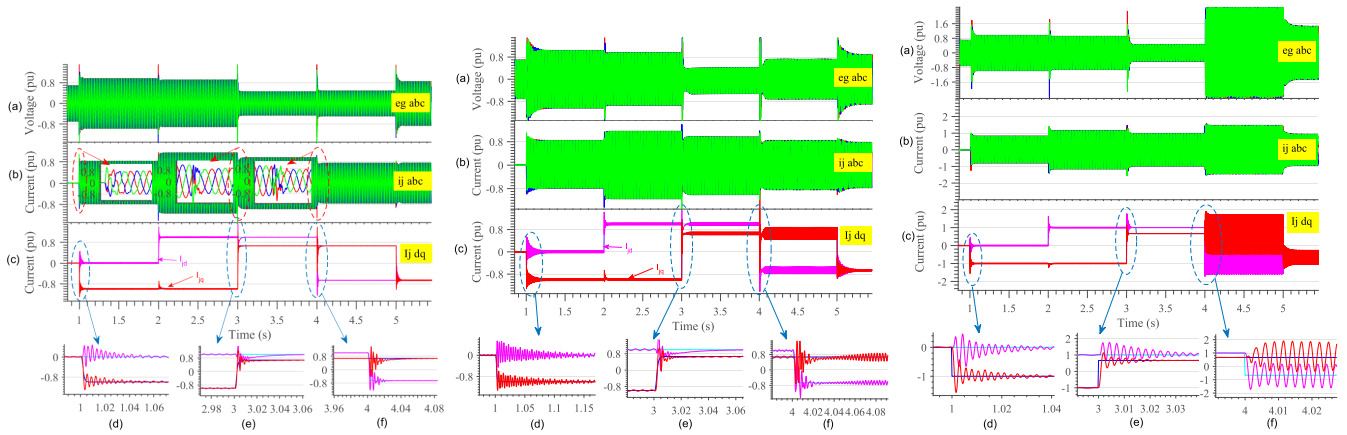


**FIGURE 10.** Simulation results for weaker grid with step in active and reactive currents; FBC with SCR of 1.4 (left plot), FBC with SCR of 1.1 (middle plot) and GPI with SCR of 1.4 (right plot).

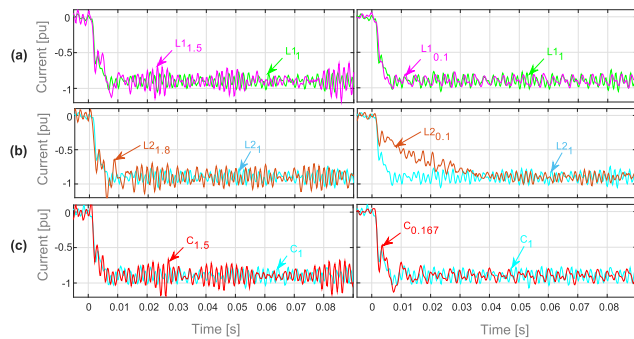


**FIGURE 11.** Simulation results: a step in  $q$ -component of injected current ( $I_q$ ) for inaccurate knowledge of system parameters (a)  $L_{r1}$ , (b)  $L_{r2}$  and (c)  $C_f$ .

As the SCR reduces to 1.4, the GPI becomes unstable at  $t = 4$  s: this instability is due to PLL and controller interaction. To avoid such a situation, either the PLL or the current controller bandwidth must be reduced which will compromise the dynamic performance, such case has been explained in [43], on the other hand, the proposed FBC controller remains stable with an overshoot equal to 0.3 and a slight increase in settling time. Further weakening the grid by decreasing the SCR to 1.1, results in an oscillatory behavior of FBC at  $t = 4$  s. This is due to the low passive damping in the low frequency region as explained in section III-B. Simulation results have shown the robustness of the proposed FBC even for very weak grid condition. The results for different values of SCR are summarized in Table 2.

#### 5) SENSITIVITY TO PARAMETER VARIATION FOR FBC

As the filter resistance, inductance and capacitance are not known with good accuracy, the estimated values for the filter ( $R_{r1}$ ,  $R_{r2}$ ,  $L_{r1}$ ,  $L_{r2}$  and  $C_f$ ) are used in the equations of the controller. Since the resistance is almost negligible compared to reactance, the system response is considered insensitive to  $R_{r1,2}$ . Fig. 11(a) shows the  $q$ -component of the injected current  $I_q$  in p.u. for  $L_{r1} = 2$  mH, when the

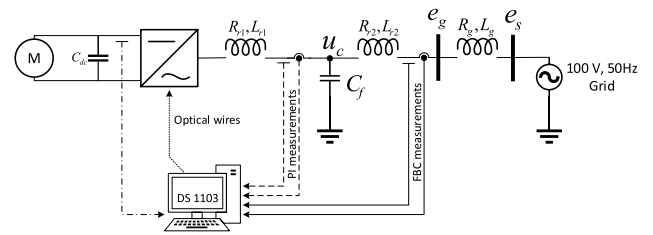


**FIGURE 12.** Single line diagram of the laboratory setup.

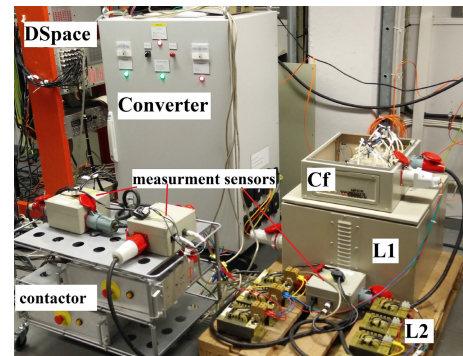


**FIGURE 13.** Experimental setup.

filter inductance varies within [0.1 to 1.5] p.u. It can be noted that the system remains stable but with more oscillations around the higher estimated inductance values. In the case of filter inductance  $L_{r2}$  (in p.u. of  $L_{r2} = 2$  mH), oscillations increase significantly for overestimation above 1.8 p.u., while underestimation slows down the response time (Fig. 11(b)). When filter capacitor value varies from 0.165 to 1.5 p.u., oscillations appear only for overestimation (Fig. 11(c)). So, the system appears less sensitive to the underestimation of filter parameters.

## V. EXPERIMENTAL RESULTS

The experimental verification of the proposed FBC and a comparison to GPI and CPI based vector current control are



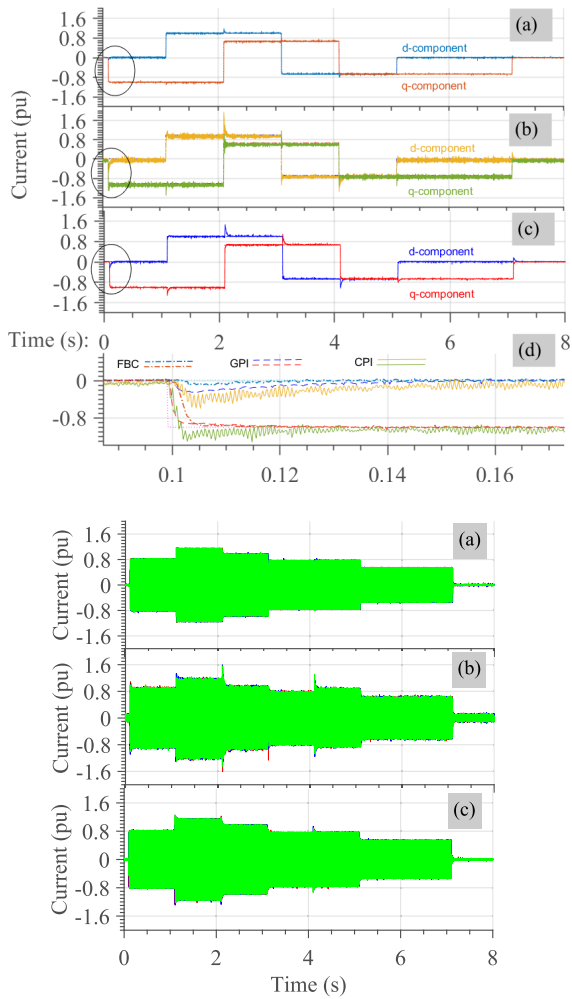


**FIGURE 14.** Experimental results for a step-change in injected current at the PCC with SCR of 8.6 (strong grid). Measured  $dq$ -components of current (top plot) and three-phase currents (bottom plot); a step in injected current at the PCC for  $dq$ -component of current for FBC (a), CPI (b), GPI (c) and zoomed transient response at 0.1 s (d).

presented in this section. In these tests,  $L_g$  is varied from 2 to 15 mH, corresponding to stiff grid condition till very weak condition with SCR from 34 to 1.1, respectively. Setup parameters are reported in Table 1. The single line diagram of the experimental setup is given in Fig. 12. The VSC is controlled from a computer with a dSpace® 1103 board, that has a 20 MHz TMS320F240 slave DSP. The DC-link of the VSC is connected to a DC machine rated 700 V and 60 A, which gives the VSC active power injection capability. The terminal voltage of the DC machine is taken to the constant value of 400 V and this arrangement has been maintained during the whole section of tests. The complete laboratory setup is shown in Fig. 13.

**A. CASE 1: DYNAMIC PERFORMANCE OF CURRENT CONTROLLERS UNDER STRONG GRID**

To test and compare the different system dynamic responses, all three controllers have been set to the same bandwidth. Note that a negative  $d$  or  $q$  component of the current injects

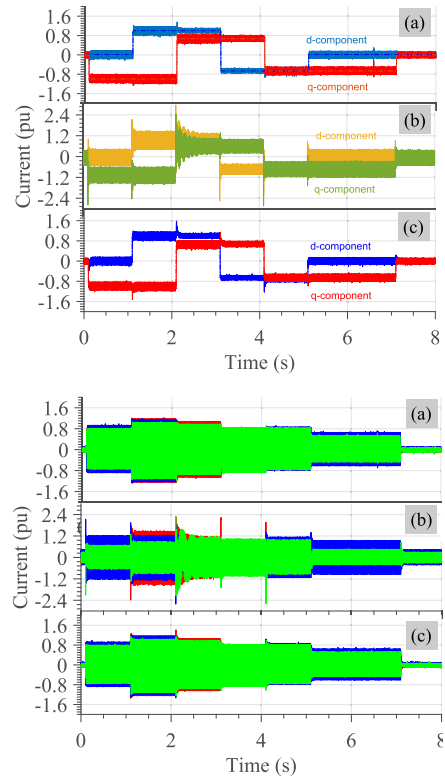


**FIGURE 15.** Experimental results with grid voltage unbalance of 10% and SCR of 1.7 (weak grid). Measured PCC current  $dq$  components (top plot) and three-phase currents (bottom plot); a step in injected current at the PCC for  $dq$ -component of FBC (a), CPI (b) and GPI (c).

either active or reactive power into the grid, respectively. Fig. 14, shows the step in  $dq$ -components of injected current at the PCC. Notice that the FBC follows its corresponding reference trajectory, smoother than CPI and GPI controllers, which exhibits some oscillations during the transient along with overshoots. Compared to simulation, the overshoot is smaller in the experimental results due to additional damping in the practical system (e.g. resistance of the devices and wiring connections).

**B. CASE 2: DYNAMIC PERFORMANCE OF CURRENT CONTROLLERS UNDER UNBALANCE GRID VOLTAGE**

As the grid is often unbalanced, according to standards, all controllers should be able to handle unbalances at least 10%. Therefore, the controllers were tested under an unbalance of 10% in the grid voltage. As can be seen in Fig. 15, the  $dq$ -components of the PCC currents are affected by 100 Hz oscillation. This affects all three controllers as shown in Figs. 15 (a)-(c). However, the CPI controller is influenced more as compared to both the GPI and FBC, as it controls the filter reactor current  $I_r$  that is less smoothed than  $I_j$ .

**C. CASE 3: DYNAMIC PERFORMANCE OF CURRENT CONTROLLERS UNDER WEAK GRID CONDITION**

Grid inductance  $L_g$  is varied from 10 mH to 15 mH which corresponds to the SCR ratio from 1.7 to 1.1, respectively. Fig. 16 (a), (b) and (c), show the  $dq$ -component of injected

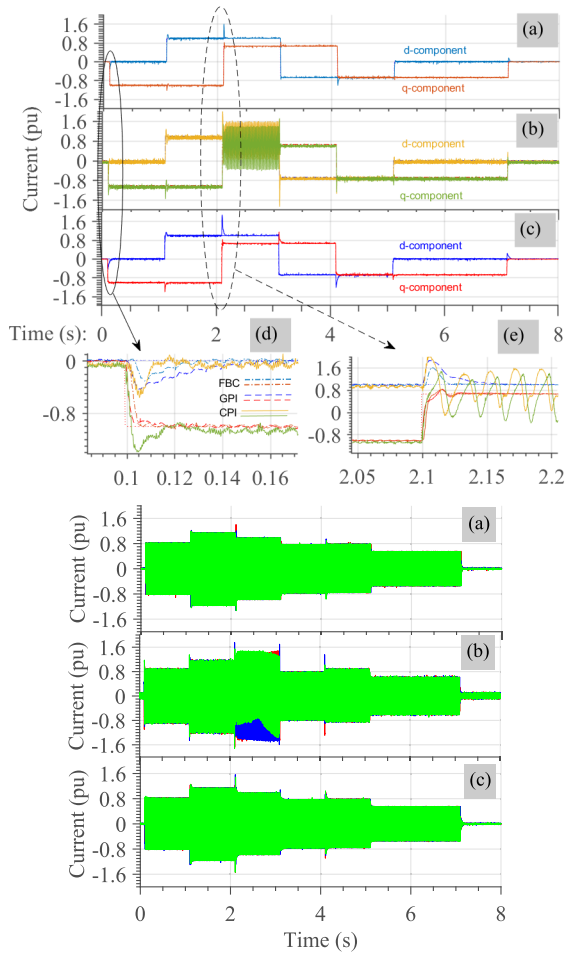


**FIGURE 16.** Experimental results with SCR of 1.7 (weak grid). Measured PCC current  $dq$ -components (top plot) and three-phase (bottom plot); a step in injected current at the PCC for  $dq$ -component of FBC (a), CPI (b), GPI (c), zoomed response at 0.1 s (d) and zoomed response at 2.1 s (e).

current for the FBC, CPI and GPI controllers. As the SCR ratio decreases up to 1.7, the grid becomes weak and the PCC voltage starts to get affected by its own injected current, making a closed-loop, as discussed in Section IV. Such a scenario may occur as reported in [44]. This condition has made the CPI controller oscillate at  $t = 2.1$  s which may easily lead to instability and can be observed in Fig. 16 (b). On the contrary, both the FBC and GPI present overshoot at  $t = 2.1$  s, with the GPI presenting twice than FBC, moreover, as shown in Fig. 16 (d) and (e), FBC has improved transient response currents.

As the grid becomes weaker ( $SCR = 1.4$ ), the FBC remains stable with a slight increase in overshoot at  $t = 2.1$ s, the GPI, instead, becomes unstable as shown in Fig. 17 (a) and (c), respectively. A reduction of the SCR below 1.1 brings FBC to become unstable, which is due to the reduced damping in the low frequency region as discussed in section III-B. Hence, the proposed FBC controller improves both stability and transient performance over the GPI controller, especially in the weaker grid conditions. The robustness of the FBC

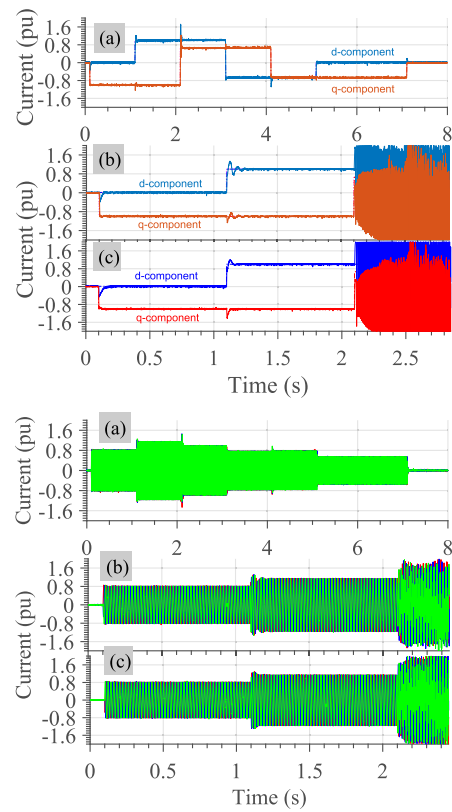


**FIGURE 17.** Experimental results for weaker grid. Measured PCC current  $dq$ -components (top plot) and three-phase (bottom plot); a step in injected current at the PCC for  $dq$ -component of FBC at SCR of 1.4 (a), FBC at SCR of 1.1 (b), and GPI at SCR of 1.4 (c).

is a direct consequence of its open-loop control structure, thus, resulting in a better trajectory tracking, as explained in previous sections.

## VI. CONCLUSION

In this paper, a novel flatness-based controller for shunt-connected VSC with LCL-filter is proposed. It provides a single-loop control solution using the grid-side current. Its performance has been compared with converter-side and grid-side VCC-based PI controllers. The simulation and experimental results confirm the performance of the proposed controller, which outperforms both controllers in terms of tracking speed, robustness to the parameter and grid impedance variations. For weak grids, the proposed FBC improves the dynamic performance and robustness of single-loop PI controller that eventually become unstable due to an increase in grid impedance.

## REFERENCES

- [1] P. A. J. Stecanella, D. Vieira, M. V. L. Vasconcelos, and A. D. L. F. Filho, "Statistical analysis of photovoltaic distributed generation penetration impacts on a utility containing hundreds of feeders," *IEEE Access*, vol. 8, pp. 175009–175019, 2020.
- [2] T. Aziz and N. Ketjoy, "PV penetration limits in low voltage networks and voltage variations," *IEEE Access*, vol. 5, pp. 16784–16792, 2017.
- [3] M. Sigle, W. Liu, and K. D. Karlsruhe, "On the impedance of the low-voltage distribution grid at frequencies up to 500 kHz," in *Proc. IEEE Int. Symp. Power Line Commun. Appl.*, Mar. 2012, pp. 30–34.

- [4] S. Jayalath and M. Hanif, "Generalized LCL-filter design algorithm for grid-connected voltage-source inverter," *IEEE Trans. Ind. Electron.*, vol. 64, no. 3, pp. 1905–1915, Mar. 2017.
- [5] R. Guzman, L. G. de Vicuna, J. Morales, M. Castilla, and J. Miret, "Model-based active damping control for three-phase voltage source inverters with LCL filter," *IEEE Trans. Power Electron.*, vol. 32, no. 7, pp. 5637–5650, Jul. 2017.
- [6] V. Miskovic, V. Blasko, T. M. Jahns, A. H. C. Smith, and C. Romanesko, "Observer-based active damping of LCL resonance in grid-connected voltage source converters," *IEEE Trans. Ind. Appl.*, vol. 50, no. 6, pp. 3977–3985, Nov. 2014.
- [7] R. N. Beres, X. Wang, F. Blaabjerg, M. Liserre, and C. L. Bak, "Optimal design of high-order passive-damped filters for grid-connected applications," *IEEE Trans. Power Electron.*, vol. 31, no. 3, pp. 2083–2098, Mar. 2016.
- [8] J. Dannehl, F. W. Fuchs, and P. B. Thøgersen, "PI state space current control of grid-connected PWM converters with LCL filters," *IEEE Trans. Power Electron.*, vol. 25, no. 9, pp. 2320–2330, Sep. 2010.
- [9] A. G. Yepes, F. D. Freijedo, O. Lopez, and J. Doval-Gandoy, "Analysis and design of resonant current controllers for voltage-source converters by means of Nyquist diagrams and sensitivity function," *IEEE Trans. Ind. Electron.*, vol. 58, no. 11, pp. 5231–5250, Nov. 2011.
- [10] Y. Tian, P. C. Loh, F. Deng, Z. Chen, and Y. Hu, "DC-link voltage coordinated-proportional control for cascaded converter with zero steady-state error and reduced system type," *IEEE Trans. Power Electron.*, vol. 31, no. 4, pp. 3177–3188, Apr. 2016.
- [11] X. Wang and F. Blaabjerg, "Harmonic stability in power electronic-based power systems: Concept, modeling, and analysis," *IEEE Trans. Smart Grid*, vol. 10, no. 3, pp. 2858–2870, May 2019.
- [12] Y. Gui, X. Wang, H. Wu, and F. Blaabjerg, "Voltage-modulated direct power control for a weak grid-connected voltage source inverters," *IEEE Trans. Power Electron.*, vol. 34, no. 11, pp. 11383–11395, Nov. 2019.
- [13] A. Adib, B. Mirafzal, X. Wang, and F. Blaabjerg, "On stability of voltage source inverters in weak grids," *IEEE Access*, vol. 6, pp. 4427–4439, 2018.
- [14] J. Roldan-Perez, E. J. Bueno, R. Pena-Alzola, and A. Rodriguez-Cabero, "All-pass-filter-based active damping for VSCs with LCL filters connected to weak grids," *IEEE Trans. Power Electron.*, vol. 33, no. 11, pp. 9890–9901, Nov. 2018.
- [15] R. P. Vieira, L. T. Martins, J. R. Massing, and M. Stefanello, "Sliding mode controller in a multiloop framework for a grid-connected VSI with LCL filter," *IEEE Trans. Ind. Electron.*, vol. 65, no. 6, pp. 4714–4723, Jun. 2018.
- [16] H. Liu, L. Li, Y. Liu, D. Xu, and Q. Gao, "Passivity based damping design for grid-connected converter with improved stability," *IEEE Access*, vol. 7, pp. 185168–185178, 2019.
- [17] X. Zhou and S. Lu, "A novel inverter-side current control method of LCL-filtered inverters based on high-pass-filtered capacitor voltage feedforward," *IEEE Access*, vol. 8, pp. 16528–16538, 2020.
- [18] Z. Xie, Y. Chen, W. Wu, Y. Xu, H. Wang, J. Guo, and A. Luo, "Modeling and control parameters design for grid-connected inverter system considering the effect of PLL and grid impedance," *IEEE Access*, vol. 8, pp. 40474–40484, 2020.
- [19] X. Fu and S. Li, "Control of single-phase grid-connected converters with lcl filters using recurrent neural network and conventional control methods," *IEEE Trans. Power Electron.*, vol. 31, no. 7, pp. 5354–5364, 2016.
- [20] K. Elyalaoui, M. Ouassaid, and M. Cherkaoui, "Improvement of THD performance of a robust controller for grid-side energy conversion system based on LCL filter without RC sensor," *Int. J. Electr. Power Energy Syst.*, vol. 121, Oct. 2020, Art. no. 106143. [Online]. Available: <http://www.sciencedirect.com/science/article/pii/S0142061519337007>
- [21] N. Pankaj, "Performance analysis of grid connected photovoltaic system with fuzzy logic control based VSC," *J. Adv. Res. Dyn. Control Syst.*, vol. 10, pp. 1439–1452, 2018.
- [22] D. Yang and X. Wang, "Unified modular state-space modeling of grid-connected voltage-source converters," *IEEE Trans. Power Electron.*, vol. 35, no. 9, pp. 9700–9715, Sep. 2020.
- [23] S. Rezaee, A. Radwan, M. Moallem, and J. Wang, "Voltage source converters connected to very weak grids: Accurate dynamic modeling, small-signal analysis, and stability improvement," *IEEE Access*, vol. 8, pp. 201120–201133, 2020.
- [24] J. Levine, *Analysis and Control of Nonlinear Systems: A Flatness-Based Approach*. Springer, 2009. [Online]. Available: <https://www.springer.com/gp/book/9783642008382>
- [25] H. Irshchik, M. Krommer, and A. K. Belyaev, Eds., *Advanced Dynamics and Model-Based Control of Structures and Machines*, vol. 13. Springer, 2012. [Online]. Available: <https://www.springer.com/gp/book/9783709107966>
- [26] A. Shahin, H. Moussa, I. Forrissi, J. P. Martin, B. Nahid-Mobarakkeh, and S. Pierfederici, "Reliability improvement approach based on flatness control of parallel-connected inverters," *IEEE Trans. Power Electron.*, vol. 32, no. 1, pp. 681–692, Jan. 2017.
- [27] R. Sherick and R. Yinger, "Modernizing the California grid: Preparing for a future with high penetrations of distributed energy resources," *IEEE Power Energy Mag.*, vol. 15, no. 2, pp. 20–28, Mar. 2017.
- [28] L. Gil-Antonio, B. Saldivar, O. Portillo-Rodríguez, G. Vázquez-Guzmán, and S. M. De Oca-Armeaga, "Trajectory tracking control for a boost converter based on the differential flatness property," *IEEE Access*, vol. 7, pp. 63437–63446, 2019.
- [29] J. R. García-Sánchez, E. Hernández-Mirquez, J. Ramírez-Morales, M. Marciano-Melchor, M. Marcelino-Aranda, H. Taud, and R. Silva-Ortigoza, "A robust differential flatness-based tracking control for the 'MIMO DC/DC boost converter-inverte-DC motor' system: Experimental results," *IEEE Access*, vol. 7, pp. 84497–84505, 2019.
- [30] A. Houari, H. Renaudineau, J.-P. Martin, S. Pierfederici, and F. Meibody-Tabar, "Flatness-based control of three-phase inverter with output LC filter," *IEEE Trans. Ind. Electron.*, vol. 59, no. 7, pp. 2890–2897, Jul. 2012.
- [31] E. Song, A. F. Lynch, and V. Dinavahi, "Experimental validation of nonlinear control for a voltage source converter," *IEEE Trans. Control Syst. Technol.*, vol. 17, no. 5, pp. 1135–1144, Sep. 2009.
- [32] Y. Xu, F. Li, Z. Jin, and C. Huang, "Flatness-based adaptive control (FBAC) for STATCOM," *Electr. Power Syst. Res.*, vol. 122, pp. 76–85, May 2015. <http://www.sciencedirect.com/science/article/pii/S0378779614004696>
- [33] C. Buccella, H. A. Khalid, C. Cecati, and D. Xu, "On flatness-based controller for shunt-connected VSC with LCL-filter for voltage dip mitigation in a weak grid," in *Proc. IECON 41st Annu. Conf. IEEE Ind. Electron. Soc.*, Nov. 2015, pp. 005062–005067.
- [34] L. Harnefors and H.-P. Nee, "Model-based current control of AC machines using the internal model control method," *IEEE Trans. Ind. Appl.*, vol. 34, no. 1, pp. 133–141, Jan. 1998.
- [35] L. Harnefors, L. Zhang, and M. Bongiorno, "Frequency-domain passivity-based current controller design," *IET Power Electron.*, vol. 1, no. 4, pp. 455–465, Dec. 2008.
- [36] C. Wang, K. Yuan, P. Li, B. Jiao, and G. Song, "A projective integration method for transient stability assessment of power systems with a high penetration of distributed generation," *IEEE Trans. Smart Grid*, vol. 9, no. 1, pp. 386–395, Jan. 2018.
- [37] M. Fliess, J. Lévine, P. Martin, and P. Rouchon, "Flatness and defect of non-linear systems: Introductory theory and examples," *Int. J. Control*, vol. 61, no. 6, pp. 1327–1361, Jun. 1995.
- [38] H. Sira-Ramirez and M. A. Oliver-Salazar, "On the robust control of buck-converter DC-motor combinations," *IEEE Trans. Power Electron.*, vol. 28, no. 8, pp. 3912–3922, Aug. 2013.
- [39] C. Buccella, C. Cecati, H. A. Khalid, and A. Ul-Haq, "On flatness-based control for series-connected VSC for voltage dip mitigation," in *Proc. IEEE 23rd Int. Symp. Ind. Electron. (ISIE)*, Jun. 2014, pp. 2637–2642.
- [40] J. Xu, Q. Qian, B. Zhang, and S. Xie, "Harmonics and stability analysis of single-phase grid-connected inverters in distributed power generation systems considering phase-locked loop impact," *IEEE Trans. Sustain. Energy*, vol. 10, no. 3, pp. 1470–1480, Jul. 2019.
- [41] S. Golestan and J. M. Guerrero, "Conventional synchronous reference frame phase-locked loop is an adaptive complex filter," *IEEE Trans. Ind. Electron.*, vol. 62, no. 3, pp. 1679–1682, Mar. 2015.
- [42] L. Harnefors, M. Bongiorno, and S. Lundberg, "Input-admittance calculation and shaping for controlled voltage-source converters," *IEEE Trans. Ind. Electron.*, vol. 54, no. 6, pp. 3323–3334, Dec. 2007.
- [43] L. Angquist and M. Bongiorno, "Auto-normalizing phase-locked loop for grid-connected converters," in *Proc. IEEE Energy Convers. Congr. Expo.*, Sep. 2009, pp. 2957–2964.
- [44] Y. Gui, X. Wang, F. Blaabjerg, and D. Pan, "Control of grid-connected voltage-source converters: The relationship between direct-power control and vector-current control," *IEEE Ind. Electron. Mag.*, vol. 13, no. 2, pp. 31–40, Jun. 2019.



**HASSAN ABDULLAH KHALID** received the B.E. degree in electrical engineering from Air University, Islamabad, Pakistan, in 2007, the M.Sc. degree in electrical power engineering from the Chalmers University of Technology, Gothenburg, Sweden, in 2010, and the Ph.D. degree from the University of L'Aquila, L'Aquila, Italy, in 2016. Since 2016, he has been with the National University of Science and Technology, Islamabad, where he is currently an Assistant Professor. His current research interests include systems control with applications in power electronics, energy conversion, renewable energy, and smart grids.



**CARLO CECATI** (Fellow, IEEE) received the Dr.-Ing. degree in electrotechnical engineering from the University of L'Aquila, L'Aquila, in 1983. Since then, he has been with the University of L'Aquila, where he is currently a Professor of industrial electronics and drives. From 2015 to 2017, he was a Qianren Talents Professor (1000 Talents Program Distinguished Professor) with the Harbin Institute of Technology, Harbin, China. He is currently the Chief Technical Officer with

DigiPower srl., a research and development company, active in the field of power electronics. His primary research interests include power electronics, distributed generation, e-transportation, and smart grids. He was a co-recipient of the 2012 and 2013 Best Paper Award from the IEEE TRANSACTIONS ON INDUSTRIAL INFORMATICS, the 2012 Best Paper Award from the *IEEE Industrial Electronics Magazine*, and the 2019 Outstanding Paper Award from the IEEE TRANSACTIONS ON INDUSTRIAL ELECTRONICS. In 2017, he received the Antony J. Hornfeck Award from the IEEE Industrial Electronics Society and the title of "Commander of the Republic of Italy" from the President of the Republic of Italy, in 2019. From 2013 to 2015, he was the Editor-in-Chief of the IEEE TRANSACTIONS ON INDUSTRIAL ELECTRONICS.



**NASSER AHMED AL-EMADI** (Member, IEEE) received the B.Sc. and M.Sc. degrees in electrical engineering from Western Michigan University, Kalamazoo, MI, USA, in 1989 and 1994, respectively, and the Ph.D. degree in power system from Michigan State University, East Lansing, MI, USA, in 2000. He is currently the Assistant Vice President of Faculty Affairs, Qatar University, Doha, Qatar, where he is also an Associate Professor with the Department of Electrical Engineering. He has published widely in international conferences and journal papers in his field of expertise. His current research interests include electric power systems, control, protection, and in control of multiphase motor drives, renewable energy sources, and smart grid. He is a Founding Member of the Qatar Society of Engineers and served as the Advisory Board of the IEEE Qatar Section.



**ADEL GASTLI** (Senior Member, IEEE) received the B.Sc. degree in electrical engineering from the National School of Engineers of Tunis, Tunisia, in 1985, and the M.Sc. and Ph.D. degrees in electrical and computer engineering from the Nagoya Institute of Technology, Japan, in March 1990 and March 1993, respectively. From September 1985 to September 1987, he worked with the National Institute for Standards and Intellectual Property, Tunisia. From

April 1993 to July 1995, he worked with Mitsubishi Electric Corporation, Japan. He joined the Department of Electrical and Computer Engineering, Sultan Qaboos University, Oman, in August 1995, where he served as the Head of the Department, from September 2001 to August 2003 and from September 2007 to August 2009. From February 2010 to January 2013, he was the Director of Quality Assurance Office, Sultan Qaboos University. In February 2013, he joined the Department of Electrical Engineering, Qatar University, as a Professor and a Kahramaa-Siemens Chair in Energy Efficiency. From August 2013 to September 2015, he was the Associate Dean of Academic Affairs with the College of Engineering, Qatar University. His current research interests include energy efficiency, renewable energy, electric vehicles, and smart grid.



**LAZHAR BEN-BRAHIM** (Senior Member, IEEE) received the B.Sc. and M.Sc. degrees in electrical engineering from the National School of Engineers of Tunis, Tunisia, in 1985 and 1987, respectively, and the Ph.D. degree in electrical engineering from Yokohama National University, Yokohama, Japan, in 1991. From 1991 to 1997, he was with Toshiba Corporation, where he was engaged in research and development of power electronics and motor drive systems. Since September 1997, he has been

with the Department of Industrial Technology, College of Technology, Qatar University. He served as the Head of the Industrial Technology Department, from 1998 to 2005. In September 2005, he joined the Department of Electrical Engineering, Qatar University. He was also the Industrial Electronics Chair of RasGas Company and the Head of Electrical Engineering Department. He invented several new techniques for use in motor drives, power electronics, sensors, and related areas. These inventions are registered in more than 12 international patents. His current research interests include power electronics, renewable energy, electric vehicles, electric drives and sensor, and instrumentation. He is a member of IEE Japan. He is an Associate Editor of *Electrical Engineering* journal (Springer) and an Editor of *Electronics* journal (MDPI).

• • •